Astron. Astrophys. 326, 763–779 (1997)

ASTRONOMY
AND
ASTROPHYSICS

Metallicities of 4 blue supergiants near the Galactic centre

S.J. Smartt[1,2], **P.L. Dufton**[1], **and D.J. Lennon**[3,4]

[1] The Department of Pure and Applied Physics, The Queen's University of Belfast, Belfast BT7 1NN, Northern Ireland
[2] ING Telescopes, Apartado de Correos 368, Santa Cruz De La Palma, E-38780 Canary Islands, Spain
[3] Max-Planck-Institut für Astrophysik, Karl-Schwarzschild-Str. 1, D-85740 Garching bei München, Germany
[4] Institut Für Astronomie und Astrophysik der Universität München, Scheinerstrasse 1, D-81679 München, Germany

Received 1 July 1996 / Accepted 28 January 1997

Abstract. High resolution optical spectra of four blue supergiants (HD148422 B0.5 Ib; HD178487 B0.5 Ib; HD179407 B1 Ib, HD163522 B1 Ib) which lie within 4.5 kpc of the Galactic centre are presented. Careful differential LTE model atmosphere analyses are used to quantify the differences in photospheric metal abundances between these stars and MK spectral standards in the solar neighborhood. A detailed non-LTE model atmosphere analysis of one star (HD163522) confirms that the LTE differential abundances should be reliable, provided we use a comparison star with similar atmospheric parameters.

One star (HD148422; R_g = 4.5 kpc) has a chemical composition similar to normal nearby B-type stars while HD178487 (R_g = 4.1 kpc) shows a mild but consistent pattern of a metal enhanced atmosphere (with elements up by 0.1–0.3 dex). The other two stars HD163522 (R_g = 4.1 kpc) and HD179407 (R_g = 3.5 kpc) have significantly higher metal compositions than their standard comparison stars with abundances enhanced by 0.30–0.40 dex and 0.20–0.5 dex respectively.

All of the stars lie outside the Galactic plane (with distances in the range $0.5 < z < 1.4$ kpc) and its is likely that they all have been ejected from the disk at an earlier point in their lifetime. Their radial velocities are examined and we consider possible ejection mechanisms which constrain their regions of origin in the Galactic disk. We compare our results with the sulphur and oxygen abundances expected from studies of H II regions (Shaver et al. 1983, Simpson et al 1995) and find that for the metal rich stars, the studies are reasonably consistent, given the uncertainties in the stellar formation sites. However metallicities of the other two stars are lower than those predicted from the H II regions. We find that other elements (Mg, Al, Si, S, Fe) follow enhancement patterns similar to oxygen, in contrast to both H II studies which produce different abundance gradients for other metals. This paper, the first in a series, shows the potential of using early-type stars to determine metal abundances in regions of low extinction toward the Galactic centre, allowing an extension of the baseline for stellar abundance gradient studies.

Send offprint requests to: S.J. Smartt, at La Palma address.

Key words: B-stars – supergiants – abundances – the Galaxy: centre

1. Introduction

The study of metal abundance variations are fundamental to understanding the chemical evolution of the Milky Way. (e.g. Matteucci 1991). The composition of the interstellar medium provides a record of enrichment processes which have occurred through the nucleosynthesis of heavy elements in successive generations of stars. Of particular interest are spatial variations in elemental abundances, and abundance gradients for different elements; H II regions, early OB-type stars and planetary nebulae have all been extensively used as probes of the present day composition of the interstellar medium (see for example the review of Pagel & Edmunds 1981, Aller 1984, Rolleston et al. 1994, Smartt et al. 1996b). Such studies have mainly concentrated on regions near or beyond the solar circle as extinction towards the central regions ($R_g < 5 - 6$ kpc) makes optical investigations difficult. To date little work has been done on the Population I composition in this region, with abundance estimates usually coming from the extrapolation of gradients determined at larger galactocentric distances.

The most comprehensive investigation of large scale abundance gradients through studies of H II regions is that of Shaver et al. (1983), who analysed an extensive sample of well observed emission line nebulae and estimated abundance gradients in the region $6 < R_g < 13$ kpc (they also observed nebulae at $R_g < 6$ kpc but these results have high uncertainties associated with their analysis). Gradients were reliably derived for oxygen & argon, (both -0.07 dex kpc^{-1}), nitrogen (-0.09 dex kpc^{-1}), and sulphur & neon (-0.01 dex kpc^{-1}), with some marginal evidence for a steepening of these gradients in the inner regions. Gradients of O, Ne, S, and Ar were estimated over similar regions from planetary nebulae studies (Maciel & Koppen 1994) with values similar to that from oxygen in the H II

regions being found. Simpson et al. (1995) have used far infrared observations of H II regions to estimate gradients for nitrogen (-0.10 dex kpc^{-1}), with sulphur, neon and oxygen giving similar results (-0.08 dex kpc^{-1}) in the inner Galactic region $0 < R_g < 10$ kpc, although the inner 4 kpc is not well sampled.

Ratag et al. (1992) presented a study of planetary nebulae (PN) in the Galactic bulge and in particular have discussed their abundance distributions. There is a general problem in comparing PN abundances with those of OB-stars and H II regions in that the former may reflect earlier epochs of star formation and the large range of PN progenitor masses (and hence ages) complicates the scenario. The central bulge is a distinct component of the Galaxy probably with its own kinematic and chemical stellar population; hence assuming the bulge region to be a direct extension of the disc is over simplistic (see Bahcall et al. 1983, and the review of Frogel 1988). The PN abundances (for O, Ne, S, Ar) are about half those predicted by extrapolating the Shaver et al. gradient and hence these results are probably *not* reflective of the Galactic disc in the inner regions. The same difficulty exists in comparing Population I abundances with those of the bulge K giants in Baade's window recently analysed by McWilliam & Rich (1994). They find that the extant data on iron abundances from G and K giants within the solar circle imply a flat gradient; however this samples an earlier epoch to our present day abundances from H II regions and early-type stars. In contrast Minniti et al. (1995) have found an abundance gradient in bulge K giants within 2 kpc of the Galactic centre, with abundances at a particular distance showing a large scatter. They have argued that this may reflect the mixing of an older population with a younger metal rich component.

The studies of B-star abundances in the Galaxy have concentrated on the regions beyond the solar circle (e.g. Fitzsimmons et al. 1992, Gehren et al. 1985, Kilian-Montenbruck et al. 1994, Kaufer et al. 1994) and these stars being young Population I objects should have photospheric abundances reflective of their progenitor material. Smartt et al. (1996b) have discussed a detailed investigation of B-type stars between 10–18 kpc from the Galactic centre and found that a significant degree of scatter is superimposed on the overall trend of decreasing metallicity and that the interstellar medium abundances appear to be correlated with the spiral arm structure. The actual relation between metallicity and galactocentric distance may not adequately be described by a simple linear gradient. The advantages of using stars is that they provide the means to investigate the abundance variations of more elements than are generally observed in gaseous nebulae (as well as C, N, O, S, there are lines of Mg, Al, Si, and Fe available).

We have begun a programme to observe A & B type supergiants and B-type main-sequence stars which lie toward the Galactic centre but sit significantly out of the plane. Their relatively low extinctions (typically $0.2 < E(B-V) < 1.0$) allow high quality spectroscopic data to be gathered in the optical region (which contain most of the useful stellar absorption lines). Using model atmosphere techniques we are then able to produce reliable differential abundances for the aforementioned elements. This paper presents the observations and model atmosphere analysis of four blue supergiants which were formed in the inner regions of the Galaxy. The extended nature of their atmospheres means they are intrinsically bright ($M_v \sim 6.0$ from e.g. Walborn 1972) however the extreme atmospheric conditions means that non-LTE effects and macroscopic velocity fields become important, making them notoriously difficult to model quantitatively (see for example Lennon et al. 1991). We present abundances based on careful differential LTE model atmosphere analyses. A detailed non-LTE model atmosphere analysis is presented for one of the stars to show that these results are not seriously compromised by the assumption of LTE.

Table 1. Original photometry, spectral types, and Galactic coordinates. The photometric data is taken from Sembach et al. (1993) and references therein, and the spectral classifications listed are also from this reference. The MK types are revised in Sect. 3.1 from the high-resolution spectra

Star	MK	V	B-V	l	b
HD163522	B1 Ia	8.46	0.00	349.6°	−9.1°
HD148422	B1 Ia	8.60	+0.09	329.9°	−5.6°
HD178487	B0 Ia	8.66	+0.16	25.8°	−8.6°
HD179407	B0.5 Ib	9.41	+0.09	24.0 °	−10.4°

2. Observational data

2.1. Photometry and selection of targets

Sembach et al. (1993) have published high resolution spectra for interstellar lines toward 57 apparently distant late O and early B-type stars. We have selected 4 targets classified as early B-type supergiants which lie within $320° < l < 30°$ and $|b| < 11°$ and whose inferred galactocentric distances were less than 4 kpc. Their photometric parameters and their estimated MK spectral types (for references see Sembach et al.) are summarized in Table 1. These spectral types will be refined using our high quality optical spectra in Sect. 3.1.

2.2. Spectroscopic observations

Spectroscopic observations were taken on 4 different observing runs, as summarized in Table 2.

In July 1994, the stars HD163522, HD148422, and HD179407 were observed with the Anglo-Australian telescope (Siding Spring, New South Wales) using the UCLES échelle spectrograph along with the 79 lmm^{-1} grating and the TEK1K CCD detector. This instrumental setup gave a spectral resolution of 0.08Å full-width-half-maximum (FWHM). Two grating settings, centred on 4229Å and 4360Å gave virtually complete coverage between 3850–4950Å. On a subsequent observing run at the same telescope in June 1995, we employed exactly the same setup and observed HD179407 in the same wavelength regions. These were chosen to provide a significant number of metal absorption features and lines of both neutral and ionized helium, which are typical of blue supergiants in this temperature regime. The échelle system provides approximately 40Å of coverage within each order and is not ideally suited for observing

Table 2. Journal of observations - complete list of the observing runs during which spectroscopic data was gathered, see text (Sect. 2.2 for more details).

Star	Telescope	Date	Instrument	Resolution(Å)	Spectral Regions(Å)
HD163522	AAT	July 1994	UCLES	0.08	3840 - 4950
	AAT	August 1994	RGO	0.48	4230 - 4480
HD148422	AAT	July 1994	UCLES	0.08	3840 - 4950
	AAT	August 1994	RGO	0.48	4230 - 4480
HD178487	AAT	July 1994	UCLES	0.08	3840 - 4950
	AAT	August 1994	RGO	0.48	4230 - 4480
HD179407	AAT	June 1995	UCLES	0.08	3840 - 4950
	SAAO 1.9m	Oct 1995	ITS	1.00	4200 - 4500

the relatively broad hydrogen Balmer lines, which are crucial to the luminosity classification and the estimation of stellar surface gravity. We thus obtained further observations using the RGO spectrograph at the AAT with the 1200B grating and the TEK1K CCD to take observations between 4230–4480Å of HD163522, HD148422, & HD178487. For HD179407, observations of Hγ were taken with the 1.9m telescope at the South African Astronomical Observatory using the Image Tube Spectrograph (with the RPCS detector and the 30Å/mm grating) at a spectral resolution of 1.0Å FWHM. This was somewhat lower than that provided by the RGO spectrograph (FWHM of 0.5Å), however was sufficient for our purposes of estimating the luminosity class and surface gravity of the star.

The observational techniques were essentially the same for all the AAT data sets. The CCD observations were divided into 1200 or 1500 second frames in order to reduce the contamination of cosmic ray hits; multiple exposures were taken as necessary to ensure a suitable signal-to-noise ratio. Exposures of the Cu-Ar or the Cu-Ne arc lamps were taken between each frame to facilitate wavelength calibration with bias and flat fields taken at the end of each night. The observations of HD179407, using the RPCS were again divided into 1200 sec exposures and arcs were taken between each exposure, together with flat fields at both the start and end of the night.

The échelle data were reduced using the Image Reduction and Analysis Facility (IRAF), and the techniques were similar to those discussed in Ryans et al. (1996). The single order spectra were reduced using the STARLINK package FIGARO (Meyerdierks 1995) as discussed in Smartt et al. (1996a), where further details can be found. When in one dimensional format, all the spectra were transferred for further analysis to the STARLINK program DIPSO (Howarth et al. 1995). Normalisation was achieved by carefully selecting continuum regions free from absorption lines and fitting low order (of degree 3 or 4) polynomials through the noise. The spectral resolution of the échelle data was better than that required for these stars due to them having unblended metal absorption lines of FWHM between ∼0.6–2.6Å. Hence the spectra were re-binned to give an adequate resolution in each case which considerably improved the signal-to-noise in the continuum of each spectra (typically in the range 100-200) without degrading the dispersion.

Equivalent widths for the metal lines, non-diffuse lines of neutral helium and those of ionised helium were measured by the non-linear least square fitting of single or multiple Gaussian profiles to the normalised spectra. Each line is assigned an error estimate reflecting the reliability of the equivalent width measurement viz. a:error less than 10%, b:error less than 20%, c:error greater than 20%. These were assigned by considering the numerical error returned by the DIPSO line fitting computation and the qualitative accuracy of the profile fit. Where multiple wavelength entries occur, the feature measured was an unresolved blend and the total equivalent width is given. The hydrogen and diffuse helium lines were not measured in this manner but the normalised profiles were extracted directly for comparison with Galactic standards and with theoretical profiles. The equivalent width measurements for each star can be found in Table 3.

3. Method of analysis

The accurate and realistic modelling of the physical processes occurring in the atmospheres of blue supergiants raises several difficulties. Non-LTE effects may be evident, and velocity fields on a wide range of scales are likely to be present. The assumption of plane parallel geometry, normally assumed for stellar atmospheres is also likely to break down given the extended nature of the atmospheres.

Considering these problems we will not attempt, in this paper, to derive truly realistic physical models from which accurate absolute physical parameters and metallicities can be derived. Rather we shall attempt to quantify the differences in metal line strengths between our Galactic centre stars and relatively nearby MK spectral standards. Such an analysis relies crucially on accurately matching our Galactic centre stars to the appropriate standard i.e ensuring that both have very similar atmospheric parameters.

3.1. Classification of the spectra

Using the atlas of Lennon et al. (1992 & 1993) which presents spectra of Galactic blue supergiants from O9.5–B8, we have classified our Galactic centre stars (GCS). This atlas provides observations which have similar wavelength coverage, and

Table 3. Equivalent widths of metal lines for all the Galactic centre stars and the three standards; each measurement has been assigned error estimates as follows - a: error less than 10% - b: error less than 20% - c: error greater than 20%

Species & Line			HD192422	HD213087			HD24398
	HD148422	HD178487	B0.5 Ib	B0.5 Ib	HD179407	HD163522	B1 Ib
C II 4267.02 & 4267.27	227a	209a	115a	120a	323a	254a	201a
C II 4372.25 & 4374.27	287c	209a	–	72c	–	121c	90c
N II 3995.00	151a	154a	105c	50c	223a	222a	174a
N II 4035.08	37b	48b	31c	30c	–	48a	60b
N II 4236.86 & 4236.98	48b	55b	33c	32c	70b	65a	64b
N II 4241.18 & 4241.78	88a	90b	95c	45c	80b	90a	87b
N II 4447.03	117b	120c	75c	35c	154a	176b	100b
N II 4607.16	41b	60a	60c	–	–	80b	97b
N II 4613.87	32b	55b	–	43c	–	45c	81b
N II 4630.54	158a	208a	160c	130c	208a	201a	188a
N III 4634.14	34b	77a	57a	–	–	26c	–
N II 4803.29	59a	64a	76a	34c	111a	85a	119a
O II 3982.72	93c	125a	88c	103b	–	118a	100b
O II 4069.62 & 4069.89	392a	467a	215b	270b	852a[1]	359a	234a
O II 4072.16	261a	238a	190b	220b	–	304a	206a
O II 4075.86	313a	297a	190a	240b	360a	347a	245a
O II 4078.84	61b	60a	33c	33c	69c	65b	41b
O II 4084.65	130a	143b	70b	80b	169b	217a	91a
O II 4092.93	66c	71c	–	108a	–	73b	73b
O II 4132.80	98a	–	56c	–	–	130a	–
O II 4153.30	166a	189a	116c	163c	198a	189a	130a
O II 4156.53	42b	67b	39c	36c	–	64b	30c
O II 4185.45	109b	116a	64c	–	111b	97b	65c
O II 4189.79	142a	144a	86c	95b	145b	119a	100c
O II 4275.56 & 4277.40	221a	236c	149a	215a	329b	260a	–
O II 4294.79	40c	31c	30c	60c	–	66b	–
O II 4303.84	157a	131b	63c	88c	125c	122a	91b
O II 4317.14	272b	203b	140b	185b	460a[2]	243b	156a
O II 4319.63	267b	200b	110b	170a	–	283b	136a
O II 4345.56	182a	140a	95c	140a	–	188a	89a
O II 4347.42	112a	74a	228a[3]	240a[3]	–	156a	40c
O II 4349.43	330a	281a	–	–	–	347a	93a
O II 4351.26 & 4351.50	174a	130a	–	–	–	183a	68b
O II 4366.89	285a	198c	155a	190a	371a	276a	195a
O II 4414.90	284a	252a	236a	267b	569a[4]	337a	251a
O II 4416.97	231a	194a	221a	195b	–	274a	184a
O II 4452.37	88a	80b	46c	78b	78b	129a	74b
O II 4590.97	221a	223a	140a	175a	260a	257a	179a
O II 4595.96 & 4596.18	186a	187a	95b	195a	232a	220a	144a
O II 4609.44	106b	136a	50c	–	–	103b	70b
O II 4638.86	230a	231a	167c	206a	–	270a	205a
O II 4661.63	268a	233b	191a	220a	283a	298a	201a
O II 4673.74	70a	75b	70c	56c	371a[5]	75a	37b
O II 4676.24	274a	202b	140c	197c	–	304a	223b
O II 4699.00	101a	112a	78c	104c	–	142a	97a

Table 3. (continued)

Species & Line	HD148422	HD178487	HD192422 B0.5 Ib	HD213087 B0.5 Ib	HD179407	HD163522	HD24398 B1 Ib
O II 4705.34	143a	137a	92c	49c	176b	168a	125b
O II 4710.01	65a	60b	37c	–	–	68a	50c
O II 4906.83	79a	77a	80c	46c	82a	92a	79c
O II 4941.07	62a	55a	–	101a[6]	197b[6]	71a	61b
O II 4943.00	126a	89c	–	–	–	139a	115b
Mg II 4481.13 & 4481.33	163b	229b	150b	150a	327a	271b	219a
Al III 4512.54	–	–	–	–	–	55b	82c
Al III 4528.91 & 4529.20	65c	69c	50c	–	–	153c	122b
Si IV 4116.10	293a	333a	345a	290a	146c	232a	98a
Si III 4552.62	447a	402a	330a	420a	481a	469a	394a
Si III 4567.82	414a	359a	300b	345a	411a	438a	333a
Si III 4574.76	275a	223a	165a	190a	309a	300a	229a
Si III 4813.30	61a	68a	43c	51c	110b	92a	46b
Si III 4819.72	114a	92a	73c	84c	152a	132a	60b
Si III 4828.96	101a	82a	47c	54c	144a	152a	56b
S III 3961.55	44c	53c	–	39c	–	44c	–
S III 4284.99	162b	192b	–	–	–	174c	104c
S III 4361.53	95a	53c	38c	60c	58c	96b	30c
Fe III 4164.79	–	47c	–	39c	–	45b	49c
Fe III 4395.78	92b	85b	66c	40c	–	100a	51c

1. The lines at 4069 and 4072Å can't be resolved in HD179407, the value listed is the compsite line strength.
2. Similarly, the lines at 4317 & 4319Å can't be resolved in HD179407, and the value listed is the compsite line strength.
3. Blend of 4347, 4349 and 4351Å.
4. The lines at 4414 & 4416Å can't be resloved in HD179407, and the value listed is the compsite line strength.
5. The lines at 4673 & 4676Å can't be resloved in HD179407, and the value listed is the compsite line strength.
6. Blend of 4941, and 4943Å.

signal-to-noise as the GCS spectra described in the previous section, but is of lower resolution (0.8Å FWHM). The latter point is not significant given that we have re-binned our GCS spectra to a lower resolution to that obtained with UCLES.

We have assumed that the helium abundances in our GCS are similar to that of the standards – any deviations should become evident in the analysis of the helium lines (discussed below). The line strength of He II 4686Å has been reliably measured in each of our target stars and being very temperature sensitive was used as a primary indicator of spectral type. The other He II lines (4200 & 4542 Å) were also examined in each case, however due to the relative weakness of the 4200Å feature and the problems with metal line blending near 4542Å, they were given less weight. Simultaneously, the line strengths of the non-diffuse He I lines (3964, 4437, 4713 Å) were compared with those in the grid of standards which allowed further constraint of the spectral type. In addition, the profiles of the He I diffuse lines (4009, 4026, 4143, 4387, 4471, and 4922Å) were also matched to those of the standard stars. In the effective temperature range we are dealing with, the lines at 4026, 4387, 4471 and 4922 Å are relatively insensitive to changes in the spectral sub-type, hence closer attention was paid to matching the other lines. In general, consistent agreement was found when comparing the He I and He II lines of a particular GCS and a standard, which supports our assumption of a common helium abundance.

The Hγ line was used as an indicator of luminosity class and this profile was compared closely to those of the standards, paying particular attention to the width and shape of the wings. The final choice of spectral type and luminosity class was made purely from the qualitative and simultaneous matching of all the spectral lines mentioned above with in each case a standard star being found which consistently matched both the Hγ line profile and the helium features (see for example Fig. 1 and Table 4); notes on each star are given below. We deliberately avoided using metal line strengths or ratios in the classification since they will be affected significantly by metallicity and disentangling the effects of varying chemical composition together with varying atmospheric parameters would not be a trivial task.

Table 4. Comparison of the He II and non-diffuse He I line strengths in the Galactic centre stars and the standards. The stars in italics are the MK standards from the Lennon et al. atlas. The lines are assigned error estimates (a,b or c) as in Table 3.

Star	He II 4200Å	He II 4686Å	He I 3964Å	He I 4437Å	He I 4713Å
HD148422	34c	103a	203a	74a	288a
HD178487	63c	179a	176b	63a	296a
HD192422(B0.5 Ib)	*51b*	*140b*	*177b*	*25c*	*280a*
HD213087(B0.5 Ib)	*20c*	*148b*	*177b*	*45c*	*300a*
HD163522	29c	42b	240a	77a	278a
HD179407	29c	82c	–	54c	347a
HD24398(B1 Ib)	*23c*	*33b*	*226a*	*86a*	*294a*

The classifications seem well constrained as a match for *all* helium lines cannot be achieved when standards earlier and later than those quoted by one spectral subtype are considered. Our revised spectral types and luminosity classes can be found in Table 5.

HD148422:- A close match is obtained for the Hγ line by a standard of luminosity class Ib between B0.5 and B1.5 with higher luminosity class stars having narrower profiles. The He II line strengths (Table 4) imply that HD148422 must be earlier than B1, with a B0.5 Ib standard providing best match. However some of the He I line strengths appear slightly stronger in HD148422 than in either of the available B0.5 Ib standards and this small difference is reflected in the derived LTE effective temperatures (see Sect. 3.2).

HD178487:- An almost identical Hγ and diffuse He I line spectra exist for this star as for HD148422. Again we have matched these lines as closely as possible to the available standards and Fig. 1(e)-(h) show the similarity in the spectra of the Galactic centre star and the chosen standard of type B0.5 Ib. The equivalent width of the He II 4686 line, which is more sensitive to changes in effective temperature than the He I lines, indicates a slightly higher effective temperature than that of the B0.5 Ib standards may be appropriate for this star.

HD163522:- Excellent agreement is found for this star and the B1 Ib standard for the profiles shown in Fig. 1(i)-(l). The strength of the He II and the non-diffuse He I lines also support the B1 Ib classification.

HD179407:- There is a further complication involved when considering a classification of the spectra of this star. The metal lines have a much broader profile than any of the standards or GCS considered previously (with a FWHM $\sim$2.6Å). This may be due to either large scale velocity fields in the extended atmosphere or a larger stellar rotational velocity (or perhaps a combination of both). All profiles will to some extent be broadened which ever mechanism is present and we should be aware of this when comparing the H and He lines. Primarily we considered the line *strengths* of the He II and the non-diffuse He I lines as temperature indicators (He I 3964Å was not accurately measured due to blending difficulties with Hϵ) as these should not be affected by broadening providing blending with nearby metal lines is negligible. These indicate that a spectral type between B0.5 - B1 is appropriate with a Ib luminosity class standard providing a close match for Hγ. The wings are slightly broader in our target star than in the standard HD24398 (Fig. 1(m)), but this is to be expected given its much broader metal line spectra. The lines of He I 4009 & 4143Å were again matched reasonably well with the B1 Ib standard.

Table 5. Atmospheric parameters & revised spectral types. The typical random errors on T_{eff}, $\log g$, and [He] are $\pm$1000 K, $\pm$0.2 dex and $\pm$0.2 dex respectively. The uncertainty in ξ is discussed in Sect. 3.2

Star	Spectral Type	T_{eff}(LTE)	$\log g$(LTE)	[He](LTE)	ξ(LTE)
Galactic centre stars					
HD148422	B0.5 Ib	25 000	3.10	10.74	30
HD178487	B0.5 Ib	27 000	3.30	10.77	30
HD163522	B1 Ib	22 500	2.80	10.68	30
HD179407	B1 Ib	24 500	3.15	10.70	30
Standard galactic comparison stars					
HD213087	B0.5 Ib	26 500	3.10	10.73	30
HD192422	B0.5 Ib	26 500	3.10	10.64	30
HD24398	B1 Ib	22 000	2.90	10.70	30

3.2. LTE stellar atmospheric parameters

As discussed in Sect. 3.1, the use of a simple LTE model atmosphere approach is unlikely to yield reliable atmospheric parameters. Our main aim is to quantify differences in the metal line strengths of the GCS and the standards of the same spectral type for which LTE methods may be adequate. All theoretical models are based on the grid of line-blanketed LTE model atmospheres of Kurucz (1991) and further line formation codes based on these techniques; more details can be found in Smartt et al. (1996a)

For each GCS star and corresponding standard we used exactly the same methods for deriving the effective temperature, surface gravity, helium abundance and microturbulence (the derivation of these four quantities being interdependent). The effective temperatures and helium abundances were primarily estimated using the He I/He II ionization equilibria (using the lines He II 4686, He I 3964, 4437, 4713) and further checked by simultaneously fitting the He I diffuse lines of 4009, 4026 & 4387Å. Modelling difficulties with the lines He I 4143, 4471, and 4922Å, resulted in these lines being excluded; these profiles are not satisfactorily computed in an LTE or non-LTE regime

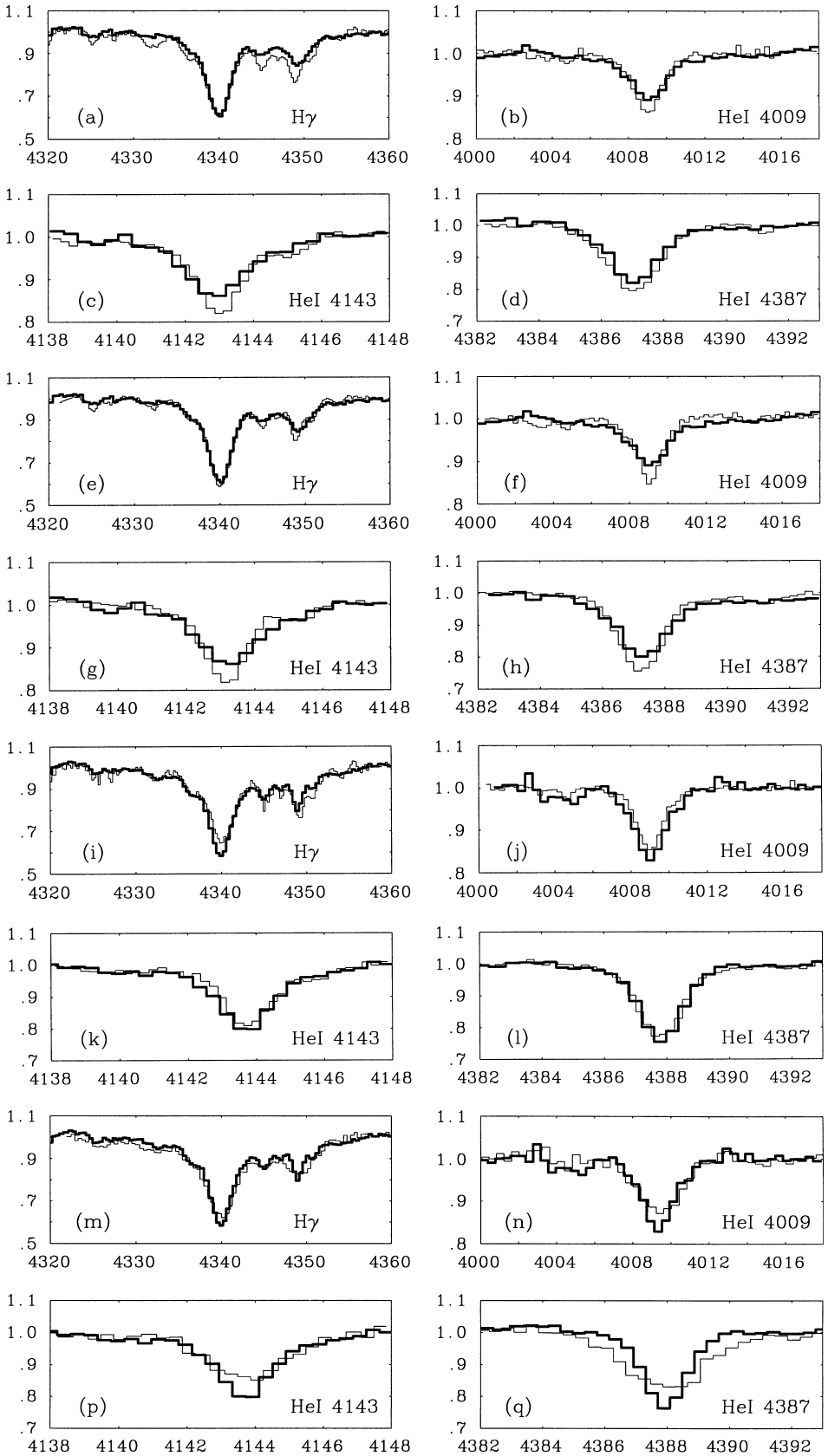

Fig. 1a–q. Examples of Hγ and He I line profiles for the Galactic centre stars and the corresponding standards of the same spectral type (in all cases the standards' spectra is the bold line). **a–d** Galactic centre supergiant HD148422 and a B0.5 Ib standard (HD213087); **e–h** Galactic centre supergiant HD178487 and a B0.5 Ib standard (HD213087); **i–l** Galactic centre supergiant HD163522 and a B1 Ib standard (HD24398); **m–q** Galactic centre supergiant HD179407 and a B1 Ib standard HD24398.

for low gravity stars (see Lennon et al. 1991), and it was not possible to match their profiles in a consistent manner.

Theoretical profiles of the gravity sensitive Hγ line were calculated using the line broadening theory of Vidal et al. (1973) and allowed the determination of log g at suitable effective temperatures. The determination of the three parameters (T_{eff}, log g, and [He]) is iterative and converged quickly in each case.

3.3. Microturbulent velocities in LTE

Microturbulence was included as an empirical fitting parameter to ensure as far as possible that no systematic trends occurred in the relation abundance vs. line strength for a given element. The estimation of this parameter relies upon having a significant number of absorption features available from the same atomic species and the spectra of O II provides the richest source of unblended metal lines in any one species. Typically 30 lines were available in each GCS and standard star (apart from HD179407 with only 12). In each case a value of between 25–35 kms^{-1} produced a near zero slope in the diagram of logarithmic abundance against equivalent width (see Fig. 2. for an example). This is a relatively large value when compared to some similar analyses of early B-type supergiants (see for example Lennon & Dufton 1986, Dufton 1979 & 1972) and represents supersonic velocities. However other LTE analyses have produced microturbulent velocities similar to the large values found here e.g Gies & Lambert (1992) show three supergiants (of types B1 Ib, B3 Iae, B2 Ib) with $\xi \sim 30\,\mathrm{kms}^{-1}$, and Van Helden (1972) analysed o^2CMa (B3 Ia) finding ξ=24 kms^{-1}. These admittedly supersonic velocities are difficult to interpret physically, however the fact that they are found in other independent analyses suggests that they are due to the LTE analyses compensating for the neglect of velocity fields on all scales as well as non-LTE effects. While these numbers may not realistically represent the microturbulent velocity fields, similar results are found in each GCS and standard, indicating that the conditions in the stellar atmospheres are comparable. Thus the differential abundances will not be seriously in error. The derived LTE atmospheric parameters of the GCS and the standards are listed in Table 5.

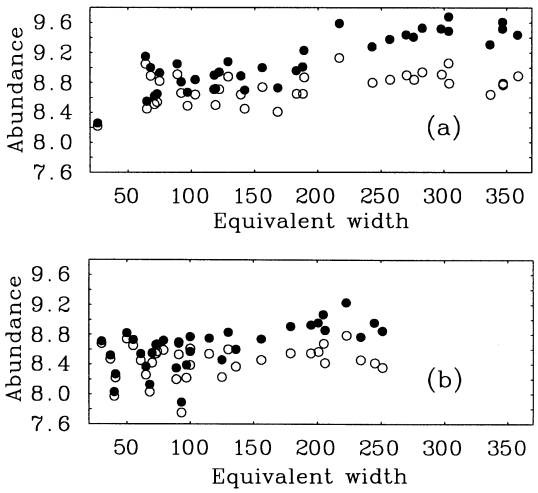

Fig. 2. a The relation between LTE logarithmic abundance and equivalent width for the O II lines of Galactic centre star HD163522. The filled symbols represent abundances calculated for ξ = 15 kms^{-1} and an obvious gradient exists. The open symbols are for ξ = 30 kms^{-1}, which indicates that derived LTE abundances are no longer dependent on line strength. **b** as for **a** but for the B1 Ib standard HD24398. A similar value for microturbulence is derived from these plots.

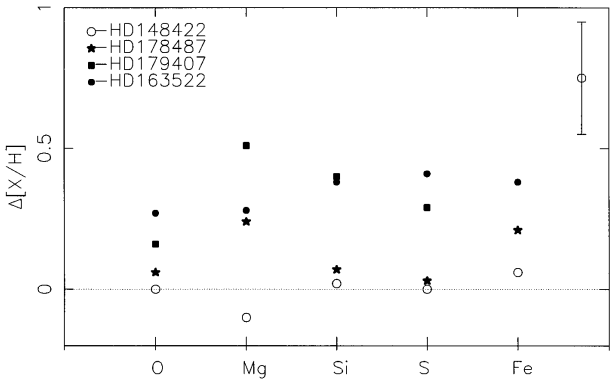

Fig. 3. Illustration of the differential metal abundances for each star, with the zero line representing the standard star metallicities. The open symbol represents HD148422, which clearly has a relatively normal chemical composition. The filled symbols representing the other stars in the study show their increased metallicity. An error bar of $\pm$0.2 dex is shown which is reflective of the typical maximum error in Tables 6–9 of the elements plotted.

4. Metal abundances from LTE differential analysis

The equivalent widths of metal lines in the spectra of the appropriate Galactic standard stars were re-measured using similar techniques to those discussed above (Sect. 2.2). The results were compared, for a consistency check with those quoted by Lennon et al. (1993) and good agreement was found. The metal line strengths are included in Table 3 for comparison purposes.

We computed LTE line blanketed model atmospheres for each star with the parameters described in Sect. 3.2. Absolute metal abundances were estimated by comparing the observed line strengths and profiles to those predicted from the model atmospheres. The atomic data used in the line formation theory were from Jeffery (1991), however this choice was not critical for our purposes of a differential analysis. A line by line differential abundance analysis was carried out for each GCS with respect to the corresponding Galactic standard (in some cases two standards were employed). Such an analysis involved estimating differential abundances for each metal line simultaneously measured in both a GCS and standard and which in both cases was judged to be relatively free from contamination due to blending from other elements. The simple mean of these results for each atomic species are quoted in Tables 6 - 9 (in each case for two values of microturbulence) with the results on a logarithmic scale, and the stars are individually discussed below. Fig. 3 illustrates the differential abundances for each element and shows the separation of the stars with different metallicity.

High resolution IUE spectra are available for the GCS and standard stars. To investigate whether these would provide additional constraints on their relative chemical compositions, spectra for HD178487 and the standard HD213087 were reduced. Particular attention was given to the wavelength region between 1890 and 1930Å that had been found by Kendall et al. (1994) to be a useful discriminant of the iron abundance. However the limited signal-to-noise ratios of the co-added IUE spectra appeared to unsuitable for investigating the modest range of metallicities in our GCS. Hence no further analysis of the IUE data was attempted.

A first and important assumption in the differential analysis is that the standard stars under consideration have a chemical composition typical of B-type stars in the solar neighbourhood. Humphreys (1978) has identified HD213087, HD192422 and HD24398 as members of the Cep OB1, Cyg OB1, and Per OB2 associations respectively. Calculations of their distances (from the MK spectral-type – absolute magnitude relation of Walborn (1972) put the stars at 1.5 kpc (HD192422), 0.9 kpc (HD213087), and 0.4 kpc (HD24398) from the Sun. From previous abundance analyses of B-type main-sequence stars, no systematic differences in metal abundance have been discovered in stars within this radial distance (Fitzsimmons et al. 1990 & 1992; Smartt et al. 1996b and references therein) It is therefore highly likely that the initial chemical composition of the standard stars are similar to normal B-type stars.

A further problem we must address is that evolutionary effects may have altered the photospheric composition (i.e. abundances of helium, carbon, nitrogen & oxygen) from that of the stars' progenitor material. Calculations regarding stellar evolution have in some cases predicted that stars in the $20M_{\odot} < M_{*} < 40M_{\odot}$ mass range may pass through a blue supergiant – red supergiant (RSG) – blue supergiant (BSG) sequence of phases (see for example Simpson 1971; Chiosi & Summa 1970; and the discussion of Fitzpatrick & Garmany 1990). During the RSG stage it is predicted that core material is mixed into the stellar atmosphere which results in CNO cycled material enriching the photospheric composition. Hence when the star returns to the BSG region of the HR-diagram its photospheric composition should indicate the presence of CNO cycled gas. One could thus envisage two BSG populations:

1. Stars with "normal" chemical composition (pre-RSG stage)
2. Stars with helium/nitrogen rich and carbon/oxygen weak atmospheres (post-RSG stage)

An alternative scenario is suggested by for example Schaller et al. (1992) who predict that the slow helium burning phase occurs immediately after the star has evolved from the main sequence and hence the "blue loops" are not predicted. Venn (1995) has shown, in a study of Galactic A-type supergiants ($5M_{\odot} < M_{*} < 20M_{\odot}$) that their non-LTE carbon and nitrogen abundances are not consistent with dredge-up having occurred in a previous red-giant phase. However their nitrogen to carbon ratios are consistent with *partial* mixing of CNO cycled gas which appears in the photosphere due to, perhaps, turbulent diffusive mixing (see Maeder 1987, Denissenkov 1994). If a similar process occurred for the B-type supergiants one would thus obtain a population whose photospheric CNO abundances had been altered since the stars birth and which would depend on the degree to which partial mixing had occurred

In either case, calculations depicting the degree to which the surface abundances are altered indicate that oxygen will not be seriously affected in either case (in general less than 0.1 dex; see Gies & Lambert 1992 and references therein). Thus in the following sections we shall discuss the abundances of oxygen, magnesium, aluminium, silicon, sulphur and iron as being the most reliable indicators of the metallicity of natal interstellar material with the carbon, nitrogen and helium abundances considered separately (see Sect. 5).

4.1. HD148422

The differential metal abundances for each observed atomic species are quoted in Table 6; where we have tabulated results using two different spectral standards (n denotes the number of lines available for use in each case). The analyses were performed using two values of microturbulence (consistently adopted in both the target stars and the standard star models). From the abundances of O II through to Fe III there is no evidence that HD148422 has a significantly different metal composition than either of the standards, particularly for a microturbulence of 30 kms^{-1}, which is our best estimate for this quantity.

Abundances differ by less than 0.1 dex compared to HD213087 apart from the Si IV result, based solely on one line which is very sensitive to temperature. Employing the standard HD192422, a difference of +0.14 dex is found for O II (assuming the larger value for microturbulence), and the Si III and Mg II values are very similar. Some variation appears with the S III and Fe III abundances and this is probably due to the limited accuracy of the line strength measurement in the standards; a statistically small number of features are available and all are designated with an error label "c". The difference in the Si IV abundance may be caused by the temperature difference of the stars, as HD192422 is slightly hotter than HD148422 and this line is extremely sensitive to effective temperature.

4.2. HD178487

In Table 7 we have tabulated the results in a similar format. When considering HD213087 as the standard comparison star there is evidence for only a marginal difference in the abundances of O II, Mg II and Si III. Using the standard HD192422, the oxygen differential abundance changes by +0.14 dex, similar to that found for the other B0.5 Ib GCS, with the Mg II and the Si III results virtually unchanged. This is similar to the pattern observed in HD148422, and indeed a differential analysis of the two standards indicates that HD213087 has an O II abundance 0.14 ± 0.13 dex higher than HD192422, with the magnesium and silicon results virtually identical. Hence this might reflect a slight deficiency in the oxygen abundance of HD192422, and the more conservative differential results using HD213087 should be given higher weight. Again, the differen-

Table 6. LTE differential abundances of HD148422 compared with HD213087(B0.5 Ib) and HD192422(B0.5 Ib)

		HD213087			HD192422	
Species	n	$\xi = 30\,\mathrm{kms}^{-1}$	$\xi = 15\,\mathrm{kms}^{-1}$	n	$\xi = 30\,\mathrm{kms}^{-1}$	$\xi = 15\,\mathrm{kms}^{-1}$
C II	2	+0.45 ±0.42	+0.73 ±0.60	1	+0.20	+0.33
N II	8	+0.07 ±0.24	+0.10 ±0.30	8	−0.18 ±0.16	−0.18 ±0.16
O II	29	0.00 ±0.16	+0.08 ±0.23	31	+0.14 ±0.15	+0.26 ±0.23
Mg II	1	−0.10	−0.10	1	−0.10	−0.10
Al III	0	—	—	1	−0.07	−0.06
Si III	6	−0.02 ±0.11	+0.06 ±0.14	6	+0.07 ±0.07	+0.22 ±0.13
Si IV	1	+0.25	+0.26	1	+0.02	−0.04
S III	2	0.00 ±0.13	+0.04 ±0.16	1	+0.32	+0.39
Fe III	1	+0.06	+0.11	1	−0.17	−0.15

tial abundances of S III and Fe III should be treated with some caution given the limitations of the observational data-set and the relative weakness of the lines in the standard spectra.

The overall conclusion, is that HD178487 shows evidence that its has a marginally but systematically higher metallicity than normal nearby B-type supergiants, and the use of two standards shows that one should be careful when considering the quantitative results.

4.3. HD179407

In Table 8, we have listed the differential abundances for HD179407, and again used two different standards. This star was classified as B1 Ib but its effective temperature estimate appears to place it between a B0.5 and B1 spectral type (see Table 5). Hence we have employed standards of both spectral types to quantify its metal composition. In general fewer unblended metal lines were available for HD179407 than for the other Galactic centre targets; the relatively broad metal lines mean many absorption features are blended with neighbouring lines. This is especially true for O II, with only 11-12 lines used in this analysis compared with approximately 30 in the other stars.

Considering first the differential analysis with respect to the standard HD24398 (B1 Ib); consistent and significant higher abundances in the species O II, Mg II, Si III, and S III imply a higher metallicity in the range 0.16–0.5 dex. Again a microturbulence of $30\,\mathrm{kms}^{-1}$ is probably the more appropriate value to use and results in a more conservative estimate of the metal enhancement. The S III result is based only on one weak line and appropriate caution should be attached to the result.

Using a B0.5 Ib as a standard (HD213087), the abundance differences are reduced somewhat, probably reflecting the inability of our models to adequately quantify variations between supergiants with even slightly different effective temperatures. The O II line strengths peak at B0.5 in blue supergiants (Lennon et al. 1993), and hence the differential results may be affected by the fact that the lines in a B0.5 Ib star are intrinsically stronger than those in a star which is a little cooler. However the two differential abundances are not significantly different given the errors on the derived values. A relatively large value for the magnesium abundance is again found even when using this standard as a comparison, illustrating the very large equivalent width measured for the 4481Å doublet in HD179407. (the abundances are again in reasonable agreement considering an expected error of ±0.2 dex inherent in the analysis methods). The discrepancy between the Si III and Si IV abundances are due to the latter's strong dependence on effective temperature; using a slightly lower effective temperature for HD179407 (by 2000 K) produces an ionization balance (with a differential value of +0.35 dex), and the differential abundances are of the other metals are changed by less than 0.1 dex.

We conclude that this object shows consistently higher abundances than normal but that their magnitude depends on the choice of standards, illustrating the limitations of our theoretical techniques.

4.4. HD163522

In Table 9 we have tabulated the results of the differential analysis of HD163522 with respect to the B1 Ib standard HD24398. For all species, a significantly higher abundance is found in HD163522, the reliable results ranging between 0.27 and 0.40 dex. There is convincing evidence for a metal rich photospheric composition, with reasonably consistent results found for each element. Oxygen has 34 lines sampled and its differential abundance (+0.27 dex) is the largest in our current dataset of stars. While the other species do not have as many observable spectral lines, they all consistently illustrate a higher than normal metallicity content; apart from aluminium which was based on two features, poorly measured in both the standard and the GCS.

There appears a large discrepancy between the Si III and the SiIV abundances which implies that the adopted effective temperature may be in error. However the differential abundance of Si IV is strongly dependent on temperature with a change of ±1000 K producing ±0.25 dex in Si IV. A balance of the ionization stages of silicon is achieved with a temperature 1000 K higher than that quoted in Table 5 and as the expected error in T_{eff} is of the order of ±1000 K this is not a serious disparity. Further, the abundances of all the other metal line species (including Si III) differ by less than ±0.07 dex with such a change in the effective temperature of either the standard or the GCS.

Table 7. LTE differential abundances of HD178487 compared with HD213087(B0.5 Ib) and HD192422(B0.5 Ib)

		HD213087			HD192422	
Species	n	$\xi = 30\,\mathrm{kms}^{-1}$	$\xi = 15\,\mathrm{kms}^{-1}$	n	$\xi = 30\,\mathrm{kms}^{-1}$	$\xi = 15\,\mathrm{kms}^{-1}$
C II	2	+0.09 ±0.29	+0.12 ±0.37	1	+0.31	+0.41
N II	8	+0.27 ±0.21	+0.32 ±0.26	8	+0.09 ±0.13	+0.11 ±0.15
O II	29	+0.06 ±0.17	+0.11 ±0.24	29	+0.20 ±0.14	+0.29 ±0.20
Mg II	1	+0.24	+0.37	1	+0.24	+0.37
Al III	0	—	—	1	+0.12	+0.14
Si III	6	+0.05 ±0.09	+0.07 ±0.11	6	+0.09 ±0.13	+0.15 ±0.22
Si IV	1	+0.19	+0.24	1	−0.04	−0.06
S III	2	+0.03 ±0.15	+0.04 ±0.16	1	+0.15	+0.16
Fe III	2	+0.21 ±0.22	+0.24 ±0.24	1	+0.35	+0.39

Table 8. LTE differential abundances of HD179407 compared with HD24398(B1 Ib) and HD213087(B0.5 Ib)

		HD24398			HD213087	
Species	n	$\xi = 30\,\mathrm{kms}^{-1}$	$\xi = 15\,\mathrm{kms}^{-1}$	n	$\xi = 30\,\mathrm{kms}^{-1}$	$\xi = 15\,\mathrm{kms}^{-1}$
C II	1	+0.56	+0.74	1	+0.36	+0.62
N II	6	+0.21 ±0.14	+0.23 ±0.18	6	+0.24 ±0.23	+0.35 ±0.29
O II	12	+0.16 ±0.10	+0.23 ±0.17	11	+0.09 ±0.13	+0.22 ±0.21
Mg II	1	+0.51	+0.72	1	+0.35	+0.63
Al III	0	—	—	0	—	—
Si III	6	+0.38 ±0.11	+0.50 ±0.11	6	+0.06 ±0.18	+0.20 ±0.19
Si IV	1	−0.15	−0.10	1	−0.17	−0.36
S III	1	+0.29	+0.31	1	−0.18	−0.17
Fe III	0	—	—	0	—	—

Table 9. LTE differential abundances of HD163522 compared with HD24398(B1 Ib)

		HD24398	
Species	n	$\xi = 30\,\mathrm{kms}^{-1}$	$\xi = 15\,\mathrm{kms}^{-1}$
C II	2	+0.26 ±0.04	+0.33 ±0.05
N II	9	+0.08 ±0.17	+0.10 ±0.22
O II	34	+0.27 ±0.21	+0.40 ±0.32
Mg II	1	+0.28	+0.38
Al III	2	+0.07 ±0.23	+0.07 ±0.28
Si III	6	+0.34 ±0.14	+0.47 ±0.15
Si IV	1	+0.62	+0.88
S III	2	+0.41 ±0.20	+0.52 ±0.10
Fe III	1	+0.38	+0.42

5. Carbon, nitrogen and helium abundances

As discussed in Sect. 4, it is possible that the photospheric abundances of carbon, nitrogen and helium in both the standard stars and the GCS may have been altered from those present in the natal material through stellar evolutionary processes.

All our stars have very similar helium abundances (see Table 5) although our estimates are consistently lower than is normal for B-stars (i.e. approximately 11.0 dex). These absolute results may be subject to certain systematic errors given our simplistic analysis methods, but the important conclusion is that there is no evidence for significant variations.

The quantitative interpretation of either the absolute or differential abundances of carbon and nitrogen presents serious problems. The two suggested evolutionary histories of blue supergiants both predict that CNO cycled gas may appear at the stellar surface, but the exact amount of this material cannot be precisely estimated given our current knowledge of the processes (see Sect. 4 above). Thus we will have two competing effects which will determine the CN composition of our GCS i.e. the natal interstellar medium abundances and the mixing mechanisms. The mixing effects may also occur in the standard stars, further complicating the picture. Disentangling the two effects to provide quantitative estimates of the original CN abundances and how they have changed through evolution for each star is not possible in this study.

We can however consider qualitatively the differential results derived and note that in general the CN differential abundances are more dependent on the choice of standard than the other elements (see, for example, the analysis of HD178487 in Table 7). Also, the CN abundances do not necessarily follow those of the other elements, indicating an additional scatter is present in the distribution alongside that present in the progenitor gas. These disparities are in qualitative agreement with the idea that some, or all, of the objects show a certain amount of CN-cycled gas at their surfaces and that the extent of this effect may vary greatly from star to star.

6. Non-LTE differential analysis of HD163522 and comparison with LTE results

As a further check on the validity of the results outlined above we have undertaken a non-LTE differential analysis of the star HD163522, in order to investigate the possibility that our results are seriously compromised by the neglect of these effects.

Table 10. Non-LTE atmospheric parameters for HD163522 and the standard HD24398. The errors on T_{eff} and log g are typically $\pm$1000 K and $\pm$0.2 dex respectively.

Star	T_{eff}	log g	[He]	ξ
HD163522	25 000	3.0	11.0	30
HD24389	25 000	3.0	11.0	30

6.1. Non-LTE model atmospheres

The non-LTE model atmospheres were computed as described in Lennon et al. (1991). The models are purely H/He, with plane parallel geometry and in hydrostatic and radiative equilibrium. The effect of wind blanketing has been ignored, however it is unlikely that this assumption will affect a *differential* analysis of the metal lines (see Lennon et al. 1991 for a discussion concerning this effect).

6.2. Atmospheric parameters

As before with the LTE model atmosphere analysis, in this section we are not concerned with estimating accurate absolute atmospheric parameters which have physical meaning. The assumption of plane parallelism and hydrostatic equilibrium are still maintained, although are of doubtful validity in supergiant analyses. Realistic derivation of the atmospheric parameters (and absolute abundances) should be dealt with by employing model atmospheres in which stellar winds, spherical extension and line blanketing are incorporated in a fully non-LTE framework. This type of analysis is not the focus of this study and here we seek only to check that the differential metal abundances previously derived are not compromised by the assumption of LTE in the model atmosphere and line formation calculations.

We have estimated the effective temperature, logarithmic surface gravity and helium abundance simultaneously as their derivation is interdependent. The method involves fitting the lines of H I, He I, and He II following similar procedures to Kudritzki (1980), and is analogous to the methods used in our LTE analysis. The He II lines used were 4200Å, & 4686Å (4542Å was ignored due to blending problems with the nearby metal lines) and being relatively insensitive to surface gravity, were the primary indicators of effective temperature. The other lines employed were Hγ, He I 4026, 4387, 4437, & 4713Å. The other observed lines of He I are not satisfactorily modelled using these model atmosphere techniques (see for example Herrero et al. 1992, and Lennon et al. 1991) and the lines listed above were considered the more reliable features for estimation of non-LTE effective temperatures and surface gravities.

In fitting each line we typically begin with Hγ and for each T_{eff} estimate a value of log g which best matches the observed profile. This gives a curve in a T_{eff} – log g diagram, with each point on the curve satisfying a fit to the observed Hγ profile. A similar procedure is followed for the other lines of He I and He II. The intersection of the loci in the T_{eff} – log g plane for these absorption lines defines the appropriate atmospheric parameters of the star. The procedure also yields an estimate of the helium/hydrogen ratio with a normal B-type star value of 0.1 by number being found to produce satisfactory fits for the stars HD163522 and the B1 Ib standard HD24398.

Table 11. Non-LTE differential abundances for HD163522 compared to HD24398; n denotes the number of lines used in both methods.

		ξ=30kms^{-1}		ξ=15kms^{-1}	
Species	n	Non-LTE	LTE	Non-LTE	LTE
N II	9	-0.02 ± 0.16	$+0.08 \pm 0.17$	-0.02 ± 0.19	$+0.10 \pm 0.22$
O II	31	$+0.30 \pm 0.17$	$+0.29 \pm 0.21$	$+0.43 \pm 0.27$	$+0.41 \pm 0.32$
Mg II	1	+0.17	+0.28	+0.21	+0.38
Si III	3	$+0.20 \pm 0.04$	$+0.24 \pm 0.05$	$+0.32 \pm 0.05$	$+0.38 \pm 0.09$
Si IV	1	+0.85	+0.62	+1.26	+0.88
S III	2	$+0.46 \pm 0.14$	$+0.41 \pm 0.20$	$+0.57 \pm 0.10$	$+0.52 \pm 0.10$

Given the similarity in the observed hydrogen and helium line spectra of these two stars, one would expect that atmospheric parameters derived using any consistent method would necessarily yield similar results. This was indeed the case in the LTE model atmosphere analysis (Sect. 3.2 above) and is also found using the non-LTE techniques. The derived atmospheric parameters are listed in Table 10. While the non-LTE temperatures are not systematically higher than their LTE counterparts by *exactly* the same percentage in each case, the disparity is only 500 K which is within the errors on each value of T_{eff} and not significantly diverse. As slightly different He I lines were used in each analysis method, this discrepancy is not serious.

6.3. Metal abundances and microturbulent velocities in non-LTE

Detailed non-LTE multilevel line formation calculations were preformed for each species of interest. The programs DETAIL and SURFACE (see Giddings 1981 and Butler 1984) were used, with the former solving the radiative transfer and statistical equilibrium equations and the latter computing the emergent flux and line profiles. The model atoms and relevant atomic data were as in Lennon et al. (1991) apart from sulphur, in which case we employed the model atom of Vrancken et al. (1996). Non-LTE curves of growth were constructed for as many of the observed absorption lines as possible using a range of abundances and microturbulent velocities of 15 kms^{-1} and 30 kms^{-1}. The results of the differential abundance analysis are summarised in Table 11, for two microturbulences with error bars referring to the mean sample standard deviation. The absence of quoted errors indicates a result based on only one line. Also included for reference are the results from the LTE differential analysis (which used exactly the same lines as were available in the non-LTE analysis).

The relation between derived abundance and line strength is shown for HD163522 and HD24398 in Fig. 4; using these two values of microturbulence. There still remains a positive gradient for ξ = 15 kms^{-1}, which disappears when ξ = 30 kms^{-1} is used. In previous non-LTE analyses of B-type supergiants, lower values of microturbulence have been found e.g. Lennon et al. (1991) adopt a value of 10 kms^{-1} in their analysis of three

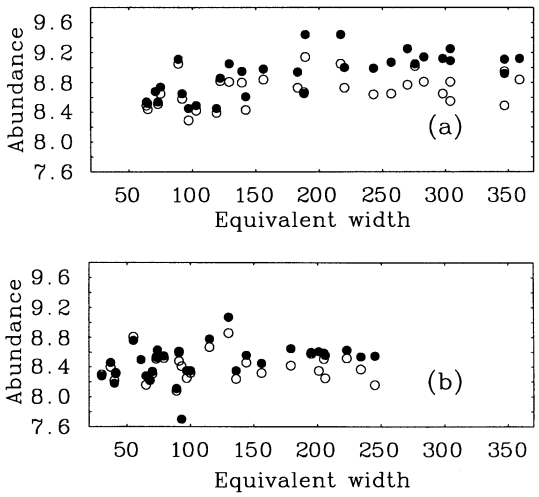

Fig. 4. a The relation between non-LTE logarithmic abundance and equivalent width for the O II lines of Galactic centre star HD163522. The filled symbols represent abundances calculated for ξ = 15 kms^{-1} and an obvious gradient exists. The open symbols are for ξ = 30 kms^{-1}, which indicates that derived non-LTE abundances are no longer dependent on line strength. **b** as for **a** but for the B1 Ib standard HD24398. A similar value for microturbulence is derived from these plots.

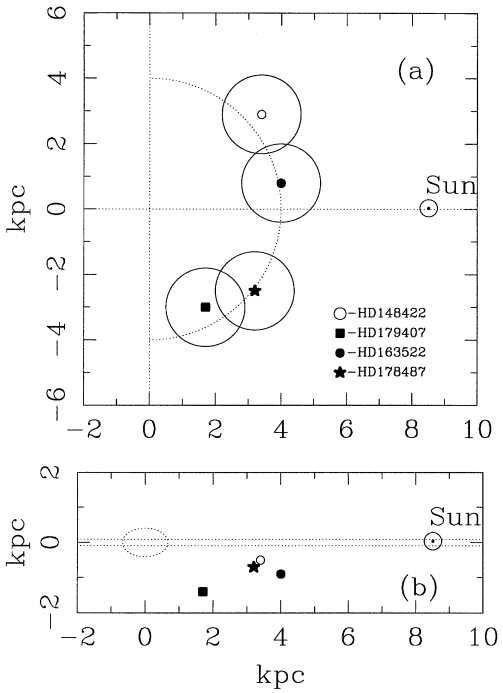

Fig. 5. a Plan view of the Galaxy with the Galactic centre at (0,0), and the Sun's position marked. The positions of the stars indicate their estimated birth sites in the Galactic disk with the error circles reflecting the uncertainties due to unknown transverse velocities and expected errors in distance calculations. The dotted semi-circle indicates the region of lower density discovered by Paczynski et al. (1994) – see Sect. 7.2. **b** Section through the Galaxy, again with the Galactic centre at (0,0). The symbols represent the stars' current positions. Also dotted is the disk (constant scale height of 90 pc) and the bulge (scale heights from Kent et al. 1991).

B0.5 Ia supergiants and Gies & Lambert (1992) find non-LTE microturbulences ∼10–15 kms^{-1} systematically lower than the corresponding LTE derivations. However one should note that the adoption of 10 kms^{-1} by Lennon et al. (using similar methods to those discussed here) did not remove the residual slope in the abundance–equivalent width plots; rather this value was adopted on the basis that larger values are supersonic and difficult to physically interpret. These analyses methods for supergiant atmospheres in the non-LTE regime are not adequate to realistically model the complete physical situation. The desaturation of metal lines could be explained by an alternative mechanism not so far included in our models e.g. photospheric outflow velocities (Kudritzki et al. 1988); which would lead to a systematic overestimate of ξ to compensate for the exclusion of this process. The important result is that similar slopes are found in the standard and GCS for a particular value of microturbulence. If we assume that a value of ξ=15 kms^{-1} is appropriate in non-LTE and that the residual slopes in the abundance–equivalent width diagram are due to another mechanism then Table 11 indicates that even then the differential results do not significantly differ from those derived using LTE and ξ=30 kms^{-1}. The scatter around the LTE (ξ=30 kms^{-1}) results is ∼0.1 dex for all ions (apart from Si IV), which is within the expected random errors quoted.

The intrinsic strength of the Si IV 4116 Å line in HD163522 (and its subsequent abundance result) implies that this star may have a higher temperature than that derived from the He I/He II line balance. The strength of this line is very temperature sensitive, and varies by a factor of approximately 2 over 2000 K in this effective temperature regime. When the ionization balance of silicon is achieved the differential abundances are changed by less than 0.1 dex (similar to Sect. 4.4 above). For all the other species good agreement exists between the LTE (ξ=30 kms^{-1}) and the non-LTE results, indicating that the differential results derived in Sect. 4 are not seriously in error due to the neglect of non-LTE effects in the atmospheres of these stars.

7. Discussion of results

7.1. Distances, Galactic positions and evolutionary status

The absolute visual magnitudes for the GCS are taken from the spectral classification – absolute magnitude calibration of Walborn (1972). As discussed in Sect. 3.1, we are confident that the adopted spectral types and (more importantly for distance estimates) luminosity classes are reliable. Walborn lists the absolute visual magnitude of Ib supergiants between types O9 – B1 as −6.0 mag. At B0.5 - B1 the range in absolute magnitude between II – Iab is ±0.5 mag., and provides an error estimate for our assumed values. The extinction for each star has been estimated using the values of $B-V$ listed in Sembach et al. (1993), and the $(B-V)_\circ$ values of Deutschman et al. (1976). The distances from the Sun ($R_\odot$) are listed in Table 12 along with the corresponding distances from the Galactic plane (z).

Given the adopted absolute magnitudes and assuming a value of -2.5 for the bolometric corrections (Code et al. 1976, Remie & Lamers 1982) we can estimate positions of the stars on the HR diagram by defining an effective temperature, compatible with that adopted in the evolutionary stellar models. The effective temperatures derived in the LTE model atmosphere analyses may not be physically realistic (see Sect. 3.2), and hence we instead adopt the effective temperature versus spectral type scale from Lennon et al. (1993). The evolutionary models of Schaller et al. (1992) predict that a star in the mass-range $20M_{\odot} \leq M_{*} \leq 25M_{\odot}$ evolves off the main-sequence in $6 \leq t_{ms} \leq 8$ Myrs, and begin a phase of core He burning which lasts a further approximately 1 Myr. During this stage the star moves across the HR diagram toward the red supergiant region. By placing our stars on the evolutionary tracks at suitable values of effective temperature and with $M_{bol} = -8.50$, we obtain an estimate of $\sim$25$M_{\odot}$ for the ZAMS mass of each star. The stars are quickly evolving in a region of fairly constant luminosity, hence the masses and lifetimes of the B0.5 Ib and the B1 Ib stars are virtually the same, and from the tracks we can approximate their current masses to be $\sim$23$M_{\odot}$. We can further infer that these stars appear to be no more than 10 Myrs old and, according to the Schaller et al. models, are burning core helium on their red-wards path. Using evolutionary models which predict different histories for stars in this mass range (e.g. Chiosi & Summa 1970 – the blue loop scenario) alters the picture of the stars movement across the HR diagram but also predicts a similar limit for the lifetimes of these stars. Additionally our conclusions (particularly regarding ages) are relatively unaffected by errors of $\pm$2000 K in the effective temperature and $\pm$0.25 mag. in the absolute bolometric magnitude.

7.2. Origins, radial velocity considerations, and Galactic structure

Our targets lie significantly below the plane of the Galaxy and it is unlikely that they have formed at their current positions. A more probable explanation is that they have been formed within the plane, and have subsequently been ejected i.e. they are runaway stars (see for example Conlon et al. 1990). In order to constrain regions of the Galactic plane from which these stars probably originated, it is necessary to assume a value for their initial velocity of ejection. Leonard (1993) has discussed mechanisms for ejecting stars from the plane of the Galaxy, making definite predictions on typical maximum velocities associated with each case. Two plausible disruption mechanisms are massive binary evolution (with $v_{max} \sim 200$ kms^{-1}) and dynamical (or cluster) ejection (with $v_{max} \sim 350$ kms^{-1}). Higher maximum ejection velocities have been predicted for early O-type stars but Leonard reports that "such extreme runaways should be extraordinarily rare". Accepting a maximum value of ejection velocity of v_{max} = 350 kms^{-1} and given the derived lifetime of the stars to be no more than 10 Myrs, we can estimate a region in the Galactic plane from which the stars could have originated. For such values of ejection velocity, the gravitational potential of the Galaxy is negligible (e.g. using a form taken from House & Kilkenny 1980 scarcely alters the conclusions below; the escape velocity from the solar neighbourhood is $\sim$360 kms^{-1}). The maximum distance travelled by each star is thus trivially 3.6 kpc in 10 Myrs. We can then define a cone whose height is defined by the perpendicular distance of the star from the Galactic plane and whose length of side is the maximum distance travelled. The base of this cone determines a circular locus in the disc within which the star must have originated. The radius of this circle (Δr_{max}) is listed in Table 12 for each star.

This region defines the *maximum* area in which a star could have originated, indeed they may have been born much closer to their point of projection of the stars' position on the plane and been ejected with a smaller velocity. The velocity distribution of runaways (calculated using either ejection mechanism) as discussed by Leonard is roughly Maxwellian with a peak at 50–100 kms^{-1}. It is quite possible then that the stars considered here had an ejection velocity much less than the 350 kms^{-1}, and we have measured their radial velocities in a further attempt to constrain their birth sites. Table 12 lists two velocities for each star; $V_{lsr\odot}$ is the radial velocity of the star with respect to the local standard of rest in the solar neighbourhood; PRV is the peculiar radial velocity of the star with respect to it's standard of rest (calculated assuming a flat galactic rotation curve and $R_{\odot}$ = 8.5 kpc, Θ = 220 kms^{-1} from Kerr & Lynden-Bell 1986) and a negative result indicates that the star is moving toward the sun.

The PRV is only one component of the peculiar space velocity with the other two components unknown (these are directed along axes mutually perpendicular to the PRV). Our PRV estimates range from 80 to 120 kms^{-1} and for illustrative purposes we shall assume that the other components of the peculiar space velocity are of the order of 120 kms^{-1}. Using the measured value of PRV we can calculate how far a star has travelled during its lifetime along the radial line of sight, allowing an estimation of it's original birthplace. Assuming that the peculiar velocity component which is perpendicular to the line of sight and effectively in the galactic plane is $\pm$120 kms^{-1} we can place uncertainty limits on this calculated position. We assume that the third velocity component is directed normal to the plane (given the small galactic latitudes of our targets, this will be a reasonable assumption). In Fig. 5(a) we show the calculated birth places of the stars with the error circles representing both the uncertainty in the transverse velocity components and the expected errors in the adopted absolute magnitudes and the extinction. Table 12 lists stars' current distance from the sun ($R_{\odot}$), the current distance below the plane (z), along with the estimated formation distance from the Galactic centre including expected uncertainties (R_g). We note that these calculations are limited somewhat by the unknown value of each separate velocity component, and we cannot unequivocally rule out the existence of larger space velocities which would imply uncertainties in the formation sites (and hence of R_g) of up to $\pm\Delta r_{max}$.

The structure of the Galaxy at these radii merits some discussion. The standard Galaxy model (Bahcall & Soneira 1980; Bahcall 1986) adopts a relation for number density of disk stars which falls off exponentially with increasing distance from the

Table 12. Distances, radial velocities and regions of origin for the stars. All distances are in kilo-parsecs and all velocities are in kms^{-1} – see text for details on each symbol.

Star	$R_\odot$	z	$V_{lsr\odot}$	PRV	R_g	Δr_{max}
HD148422	5.2	−0.5	−28	−86	4.5 ±1.2	±3.6
HD178487	4.9	−0.7	−36	−117	4.1 ±1.2	±3.5
HD179407	7.6	−1.4	−103	+26	3.5 ±1.2	±3.3
HD163522	5.6	−0.9	+35	+98	4.1 ±1.2	±3.5

Galactic centre (with scale length 3.5 kpc), and also decreases exponentially with distance from the plane (with scale height dependant on the spectral type of stars considered; approximately 90 pc for B-stars Bahcall 1986 p. 595). Hence as we progress toward the Galactic centre the number density of disk stars should increase, and we might expect the number of runaways, such as those in our sample to be more numerous than in the solar neighbourhood. However recent evidence suggests that the actual situation maybe distinctly different. First of all Kent et al. (1991) indicate that the scale height decreases toward the Galactic centre (by a factor of ∼0.67 between the solar position and R_g = 5 kpc). Secondly Paczynski et al. (1994) in a colour-magnitude study of $\sim 3 \times 10^5$ stars in Baade's Window (centred on b = −3.9°, l = 1.0°) produced the surprising result that the stellar number density is observed to be roughly uniform between us and d∼3–4 kpc (a region including the Sagittarius spiral arm) and then rapidly decreases by a factor of ∼10 beyond that distance. If this is the case then we would expect a lower number of disk stars, and hence runaways to exist in the inner 4 kpc than predicted from the standard model. Indeed it is interesting to note that the stars in this, albeit small sample, tend to avoid the inner regions (in Fig. 5(a) we have marked a semi-circle of radius 4 kpc indicating the region of possible low density from Paczynski et al. 1994). A further paper on the analysis of early type stars near the Galactic centre (including new data on B-main-sequence and A-supergiants) is in preparation and preliminary results indicate that stars again tend to lie outside this inner region. This may be purely a selection effect reflecting the limits of visual magnitude in the original photometric and spectroscopic data bases. Also the number of early-type stars seen towards the galactic centre depends upon the *current* star formation rate, whereas the sample of Paczynski et al. will be sampling this at earlier epochs. The stellar content of the inner disc is, at present, poorly understood and is worth further investigation.

7.3. Metallicity variations towards the Galactic centre

The metallicity of HD148422 appears similar to B-type stars in the solar neighbourhood. We estimate it's birth place to be 4.5 ±1.2 kpc from the Galactic centre and indicates that stars with normal abundances exist within 6 kpc of the centre. However we cannot completely discount the possibility that the star formed outside this Galactic radius and hence that the photospheric metal abundances are more typical of material at a larger galactocentric distance.

HD178487 probably formed in the disc at around R_g ∼4.1 kpc, and establishes the existence of material with slightly higher than solar abundances in the intermediate region between the Sun and the Galactic centre. We can quantitatively compare the results with those in other studies, but must keep in mind the uncertainty in the formation site. An extrapolation of the Shaver et al. (1983) gradient (for oxygen; −0.07 dex kpc^{-1}) would predict a metallicity approximately 0.31 dex higher than normal. The oxygen abundance in this star is derived as between 0.06–0.20 higher than the standards (depending on which is chosen) and is hence lower than would be expected from the H II region result. The other elements follow a similar pattern in that they are all enhanced by a marginal amount, of the same order as the oxygen differential result. The small discrepancies between the elements are probably not statistically significant given the results for these elements are based on only a few absorption lines.

The other two stars in the study show definitive evidence of higher than normal metallicities. We consider first HD163522, which has enhanced metal abundances ranging between 0.3–0.4 dex. The primary elements (O, Mg, Si, S) show a reasonably consistent pattern of enhancement as would be expected considering the nucleosynthetic history of these nuclides. Assuming its estimated galactocentric distance of 4.1 kpc then from the Shaver et al. results we would expect oxygen to be enhanced by +0.31 dex, which agrees with the current results within the expected errors. We also note that Shaver et al. have found quite different gradients for different elements (e.g. sulphur and neon show flat gradients, while argon is similar to that of oxygen). The differential abundances that we derived are consistent with the primary elements being enhanced on a similar scale i.e. magnesium, silicon, sulphur, *do* show enhancements similar to that of oxygen. Simpson et al. (1995) have found that abundance gradients from oxygen, neon and sulphur are not statistically different (approximately −0.07 dex kpc^{-1}; similar to Shaver et al.'s oxygen result) and our abundances from HD163552 support these findings

The results for HD179407 show a larger scatter than for the previously discussed stars, probably reflecting the fewer lines available for the analysis. Significantly we again notice that all the primary elements show consistent differential abundances, in accord with the results from HD163522. Given its estimated formation distance of 3.5 ±1.2 kpc from the centre we would expect abundances to be up by ∼0.3 ± 0.13 dex (from both the Shaver et al. and the Simpson et al. results), and considering the uncertainties our findings lie within the expected range.

In Fig. 6 we have compared the results of two major H II region studies of the inner Galaxy with our abundances, picking the best sampled elements complimentary to both data sets (i.e. sulphur to compare with Simpson et al. and oxygen to compare with Shaver et al.). Simpson et al. have suggested that their distribution of sulphur abundances could be statistically well matched with either a step function (abundances similar to solar for $R_g > 6$ kpc, and ∼0.37 dex above solar for $R_g < 6$ kpc) or a gradient (−0.07 dex kpc^{-1}) and in Fig. 6(a) we have plotted both of these relations, along with the stellar results. The two

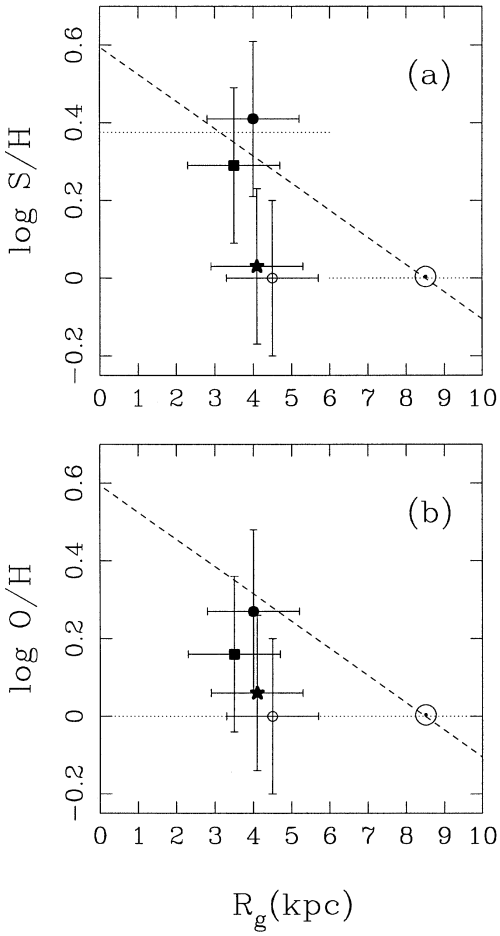

Fig. 6. a Comparison of sulphur abundances from Simpson et al. (1995) and our stellar results. The dotted horizontal lines show the "step function" discussed by Simpson et al. and the dashed line shows their derived gradient. Solar abundance is set at log $S/H = 0$ for $R_g = 8.5$ kpc and the errors on the y-scale are taken from Tables 6–9 (with a minimum of ± 0.2 dex assumed to be realistic). Stellar symbols are as in Fig. 5. **b** Comparison with oxygen abundances from Shaver et al. (1983) and our stellar results. The dashed line indicates the H II region abundance gradient. Stellar results are illustrated as in (a).

most metal rich stars (HD163522 & HD179407) are in reasonable agreement with the Simpson et al. data, within the errors, however the other stars appear to have somewhat lower abundances. We note that Shaver et al. found a very shallow gradient for sulphur, however this element was unreliable within $R_g \sim 7$ kpc, and hence we presume the more substantive results of Simpson et al. to be more reliable. Fig. 6. (b) shows the oxygen abundance gradient from Shaver et al. and our stellar results (the Simpson et al. study has only sparse data for oxygen and it produces a similar result). Our results are in general lower than the predicted H II regions apart from HD163522 & HD179407, the two most enhanced objects. A much larger sample of stars is required to clarify the situation further, as from Fig. 6 our limited data set precludes any definite conclusion regarding the comparison with H II region results. It is unclear whether the discrepancies are due to, for example, real scatter about an overall gradient, or if stellar abundances give distinctly different results to those from H II region studies. Smartt et al. (1996b) have discussed the scatter of abundances at a given galactocentric distance in the anti-centre direction and found significant deviations about the gradient implied from the H II region data. The differences could also be due to a significant steepening of metallicity gradients within the inner 4 kpc. This initial study confirms that Population I stellar abundances tend to increase near the central regions of the Galaxy. There is marginal evidence for the correlation of the iron abundance with that of oxygen (although the data set is limited). This is in conflict with the recent results from Carr et al. (1996) who suggest that the iron abundance in a Population I red supergiant at the galactic centre is similar to the solar value. Their derived mass estimate of 20–25 $M_\odot$ for this star means that it has an age of $\sim$10 Myr, and reflects the most recent starburst in the central cluster. The luminosity classification and its mass estimate from evolutionary calculations are crucial to its age determination and hence the epoch in which it formed.

7.4. Summary

We report the finding of two stars HD163522 & HD179407 near the Galactic centre with enhanced metal abundances. The metallicities are up by between 0.3–0.4 dex and 0.2–0.5 dex respectively, compared to normal near sun B-type stars and these enhancements are in reasonable agreement with results from H II region studies. HD178487 shows abundances marginally but consistently higher than in our comparison stars while HD148422 has a relatively normal chemical composition. The abundances in the latter two stars are lower than those predicted from H II region studies. The galactocentric distances at which the stars formed are somewhat uncertain given that the stars have been ejected from the plane and only one component of their space velocity can be measured. There is evidence that the primary element abundances (O, Mg, Al, Si, S) are correlated which is also in contrast to the results from the nebular investigations. We shall present further analyses of early-type stars (both B-type main-sequence, and A-type supergiants) in this region of the Galaxy in a future paper.

Acknowledgements. Observational data were obtained at the Anglo-Australian Observatory in Siding Spring, New South Wales and at the South African Astronomical Observatory in Sutherland. We are grateful to the staff at both observatories for their assistance. Data reduction was performed on the PPARC funded Northern Ireland STARLINK node, and some of the model atmosphere programs were made available through the PPARC supported Collaborative Computational Project No. 7. We acknowledge financial support for this work from the British Council and the Deutscher Akademischer Austauschdienst in the context of the British-German Academic Research Collaboration initiative. SJS holds a post-graduate studentship from the Department of Education for Northern Ireland, and would like to thank Prof. Francis Keenan for his ideas in initiating this work. We also thank Myriam Vrancken for providing us with unpublished data for sulphur and her assistance with the non-LTE computations.

References

Allen, C.W., 1983, Astrophysical Quantities, Athlone, London
Aller, L.H., 1984, Physics of Thermal Gaseous Nebulae (Dordrecht, D. Reidel)
Bahcall, J.N., Soneira, R.M., 1980, ApJS 44, 73
Bahcall, J.N., Schmidt, M., Soneira, R.M., 1983, ApJ 265, 730
Bahcall. J.N., 1986, ARA&A 24, 577
Butler, K., 1984, Ph.D. Thesis, University of London
Carr, J.S., Sellgren, K., Balachandran, S.C., 1996, in 4th ESO/CTIO Workshop on The Galactic Center, ASP Conf. Ser., *in press*
Chisoi, C., Summa, C., 1970, Ap.Sp.Sci 8, 478
Code, A.D., Davis, J., Bless, R.C., Hanbruy Brown, R., 1976, ApJ 67, 373
Conlon, E.S., Dufton, P.L., Keenan, F.P., Leonard, P.J.T., 1990, A&AS 236, 357
Denissenkov, P.A., 1994, A&A 287, 113
Deutschman, W.A., Davis, R.J., Schild, R.E., 1976, ApJ Supp. 30, 97
Dufton P.L., 1972, A&A 16, 31
Dufton P.L., 1979, A&A 73, 203
Fitzpatrick, E.L., Garmany, C.D., 1990, ApJ 363, 119
Fitzsimmons, A., Brown, P.J.F., Dufton, P.L., Lennon, D.J., 1990, A&A 232, 437
Fitzsimmons, A., Dufton, P.L., Rolleston, W.R.J., 1992, MNRAS 259, 489
Frogel, J.A., 1988, Ann. Rev. A&A 26, 51
Gehren, T., Nissen, P.E., Kudritzki, R.P., Butler, K., 1985, in Proc. ESO Workshop on Production and Distribution of CNO elements, European Southern Observatory, Garching, p 171
Giddings J.R., 1981, Ph.D. Thesis, University of London
Gies, D.R., Lambert, D.L., 1992, ApJ 387, 673
Herrero, A., Kudritzki, R.P., Vilchez, J.M., Kunze, D., Butler, K., Haser, S., 1992, A&A 261, 209
House, F., Kilkenny, D., 1980, A&A 81, 251
Howarth I.D., Murray J., Mills, D., Berry, D.S., 1995 Starlink User Notice, No.50.16
Humphreys, R.M., 1978, ApJS 38, 309
Jeffery, C.S., 1991, in: Newsletter on Analysis of Astronomical Spectra No. 16, p. 17
Kaufer A., Szeifert Th., Krenzin R., Baschek B., Wolf B., 1994, A&A 289, 740
Kendall, T.R., Conlon, E.S., Dufton, P.L., Keenan, F.P., 1994, A&A 290, 563
Kent, S.M., Dame, T.M., Fazio, G., 1991, ApJ 378, 131
Kerr, F.J., Lynden-Bell, D., 1986, MNRAS 221, 1023
Kilian-Montenbruck, J., Gehren, T., Nissen, P.E., 1994, A&A 291, 757
Kudritzki, R.P., 1980, A&A 85, 174
Kurucz, R.L., 1991, in Precision Photometry: Astrophysics of the Galaxy, ed. A.G. Davis-Philip, A.R. Upgren, & P.L. Janes (Schenectady:Davis)
Lennon, D.J., Dufton, P.L., 1986, A&A 155, 79
Lennon, D.J., Kudritzki, R.P., Becker, S.T., Butler K., Eber, F., Groth, H.G., Kunze, D., 1991, A&A 252, 498
Lennon, D.J., Dufton, P.L., Fitzsimmons A., 1992, A&AS 94, 569
Lennon, D.J., Dufton, P.L., Fitzsimmons A., 1993, A&AS 97, 559
Leonard, P. J. T., 1993, in Luminous High-Latitude stars, ed. D. Sasselov (San Francisco:ASP)
Maciel, W.J., Koppen, J., 1994, A&A 282, 43
Maeder, A., 1987, A&A 178, 159
Matteucci, F., 1991, in Frontiers of Stellar Evolution, ASP Conf. Ser. 20, ed. D.L. Lambert (San Francsico: ASP), p. 539.
McWilliam, A., Rich, M.A., 1994, ApJS 91, 749
Meyerdierks, H., 1995 Starlink User Notice, No. 86.10
Minniti, D., Olszewski, E.W., Liebert, J., White, S.D.M., Hill, J.M., Irwin, M.J., 1995, MNRAS 277, 1293
Pagel, B.E.J., Edmunds, M.G., 1981, ARA&A 19, 77
Paczynski, B., Stanek, K.Z., Udalski, A., Szymanski, M., Kaluzny, J., Kubiak, M., 1994, AJ 107, 2060
Ratag, M.A., Pottasch, S.R., Dennefeld, M., Menzies, J.W., 1992, A&A 255, 255
Remie, H., Lamers, H.J.G.L.M, 1982, A&A 105, 85
Rolleston, W.R.J, Dufton P.L., Fitzsimmons A., 1994, A&A 284, 72
Ryans, R.S.I, Hambly, N.C., Dufton, P.L, Keenan, F.P., 1996, MNRAS 278, 132
Schaller G., Schaerer, D., Meynet, G., Maeder, A., 1992, A&AS 96, 269
Sembach, K.R., Danks, A.C., Savage, B.D., 1993, A&AS 100, 107
Shaver, P.A., McGee, R.X., Newton, M.P., Danks A.C., Pottasch S.R., 1983, MNRAS 204, 53
Simpson, E.E., 1971, ApJ 165, 295
Simpson, J.P., Colgan, S.W.J., Rubin, R.H., Erickson, E.F., Hass, M.R., 1995, ApJ 444, 721
Smartt, S.J., Dufton, P.L., Rolleston, W.R.J. 1996a, A&A 305, 164
Smartt, S.J., Dufton P.L., Rolleston W.R.J., 1996b, A&A 310, 123
Talbot, R.J., Arnett, W.D., 1973, ApJ 186, 60
Van Helden, 1972, A&A 21, 209
Venn, K., 1995, ApJ 449, 839
Vidal, C.R., Copper, J., Smith, E.W., 1973, APJS 25, 37
Vrancken, M., Butler, K., Becker, S.R., 1996, A&A 311, 661
Walborn, N.R., 1972, AJ 77, 312

This article was processed by the author using Springer-Verlag LaTeX A&A style file *L-AA* version 3.